TÜBİTAK

Turkish Journal of Physics

http://journals.tubitak.gov.tr/physics/

Research Article

Turk J Phys
(2017) 41: 303 – 313

doi:10.3906/fiz-1612-15

Enhanced electro-optic modulation of $LiNbO_3$-based photonic crystal cavities with dual mode and polarization operation

Fulya BAĞCI[1,*], Gökhan KURT[1,2], Barış AKAOĞLU[1], Ekmel ÖZBAY[2,3]
[1]Department of Engineering Physics, Faculty of Engineering, Ankara University, Ankara, Turkey
[2]Nanotechnology Research Center, Bilkent University, Ankara, Turkey
[3]Department of Electrical and Electronics Engineering, Faculty of Engineering, Bilkent University, Ankara, Turkey

Received: 21.12.2016 • **Accepted/Published Online:** 07.03.2017 • **Final Version:** 05.09.2017

Abstract: A high output transmission and high quality factor, compact $LiNbO_3$-based Fabry–Perot-type photonic crystal cavity is reported that can be used in electro-optical modulators at optical communication wavelengths. The electro-optic effect is 123 times enhanced as compared to the bulk material as a result of the slow light effect. The transmission wavelength is found to depend linearly on the applied voltage with 1.2 nm/V modulation sensitivity. Moreover, an externally switchable dual mode regime with high quality factors and transmissions is realized. High transmissions and high quality factors are also obtained for both transverse-electric and transverse-magnetic polarizations simultaneously.

Key words: Photonic crystal, electro-optic modulation, slow light, quality factor

1. Introduction

Photonic crystal (PC) cavities have attracted considerable interest because of their flexible operation wavelength tunability with external physical signals and enhanced interaction of light with matter in a small modal volume [1–3]. By using different geometrical and structural approaches, various studies have been performed in order to design a PC cavity with an ultrahigh quality-factor (Q) in an ultrasmall modal volume [4–6]. Such cavity designs have the potential to find applications in several fields, i.e. low-threshold lasers [7], semiconductor quantum wells [8], optical communication and quantum information processing systems [9,10], channel add–drop functional devices [11], and nonlinear photonic elements for photonic chips [12].

The possibility of creating a strong light–matter interaction in the cavity region as a result of highly localized fields can lead to the enhancement of the nonlinear and electro-optic effects. This enhancement can further be increased by exploiting the slow light effect at the cavity resonance frequency. By the enhancement of the electro-optic and nonlinear effects, a PC cavity can lead to a significant modification in the refractive index of the material that constitutes the cavity region and, in turn, the operation wavelength can be drastically shifted.

PC cavities can be highly sensitive to changes in the refractive index of the cavity region, since the optical path of the travelling wave inside the cavity region can be made much longer than the physical length of the cavity. Considering the aforementioned features of PC cavities, it is possible to realize high-Q, small modal-volume, compact, and high throughput devices [12–15]. For instance, a lithium niobate ($LiNbO_3$) electro-optic

*Correspondence: fbagci@eng.ankara.edu.tr

modulator is experimentally exploited with two orders of magnitude enhanced electro-optic effect compared to that for the bulk $LiNbO_3$ due to operation in the slow light regime of the PC [16]. Another important issue in PC cavity-based refractive index sensors or electro-optic modulators is the sharpness of the band edges. It is reported that in order to have sharp band edges and high contrast between pass- and stop-bands like the band spectrum of infinite holes in a two-dimensional model, the holes should be sufficiently deep to overlap most of the waveguide mode [17]. By opening a shallow trench (1 to 1.5 μm) and etching holes in the bottom of this trench, sharp spectral features and high contrast between pass- and stop-bands are preserved with a sacrifice in transmission about 10%–25% for an annealed proton-exchange (APE) $LiNbO_3$ PC waveguide [17]. The efficiency of a shallow trench on the existence of high contrast, sharp band edges is also investigated for air-hole square-lattice PC in a Ti-diffused $LiNbO_3$ strip waveguide [18]. Thermal annealing is shown to provide an effective method to reduce loss in annealed proton exchanged $LiNbO_3$ PC waveguides so that a photonic band gap (PBG) with an extinction ratio of 15 dB is experimentally demonstrated [19].

PC cavities, which are basically point or line defects in PC structures, can be constructed in several ways. For example, heterostructure cavities are designed from cavity regions having different periodicities and/or lattice constants compared to those of the surrounding media [20]. Air bridge cavities consist of input/output coupling lines and a free-standing PC slab stage that is utilized for the purpose of minimizing the output plane losses by benefiting from total internal reflection [21]. Nanobeam cavities are patterned in a single line of rods/holes [22]. Fabry–Perot-type cavities can be formed by inserting two PC mirrors at both sides of the line-defect [23]. Although their construction is different, all these types of PC cavities have a common feature: only the resonance wavelengths of the cavity are allowed to be transmitted and other wavelengths of the PBG are reflected from the crystal.

In this study, we design a $LiNbO_3$-based two-dimensional Fabry–Perot-type PC cavity by removing a line of holes perpendicular to the light propagation direction. Simultaneous achievement of nearly unity power transmission and high field localization inside the cavity region are aimed as design targets. We selected $LiNbO_3$ as the host material because of its suitability of use in Pockels, nonlinear, acousto-optic, piezoelectric, and photorefractive devices due to its superior multiphysical properties. Besides having a large electro-optic coefficient, $LiNbO_3$ also exhibits low conductivity and a high relaxation time, which are favorable properties for sensing DC electric fields in space charge environments [24]. Photonic and phononic band gap maps are examined for different lattice types and geometrical parameters of a Z-cut $LiNbO_3$ PC slab [25]. It has been shown that simultaneous photonic and phononic band gaps are possible for a triangular lattice-type PC slab [25]. Very recently, electro-optic beam deflection was demonstrated by applying relatively low voltages (20 V) in $LiNbO_3$-annealed proton exchange waveguides [26].

Tunable, low-voltage, and micrometric-sized electro-optic modulators are realized in $LiNbO_3$-based PC cavities by combining the large electro-optic coefficient of $LiNbO_3$ with the slow light effect [14,16, 27–29]. We numerically demonstrate the enhancement of the electro-optic effect of $LiNbO_3$ inside the PC cavity region due to strong field localization and enhanced light–matter interaction arising from the slow light effect. Moreover, we show that it is possible to alter the Q of the cavity by changing the number of the hole columns (N) on either side of the cavity. In addition, a dual mode regime with a switchable operation wavelength can be achieved by altering the cavity length, L_C. Finally, we investigate the possibility of achieving a dual-polarization regime, where resonance peaks for both transverse magnetic (TM) and transverse electric (TE) polarization states are observed inside the photonic band gap (PBG) region, by altering the r/a ratio.

2. Structure and methods

As shown in Figure 1, a Fabry–Perot-type PC cavity, which is formed between two identical square lattice PC sections that act as side mirrors, is formed. The length of the cavity is represented by L_C and the radius and the periodicity of the holes are denoted by r and a, respectively. The host material is selected as $LiNbO_3$, which has a trigonal molecular crystal system and exhibits the Pockels effect and nonlinear optical polarizability [30]. Owing to its trigonal crystal distribution, which is known to lack inversion symmetry, $LiNbO_3$ displays optical birefringence with the application of a static or time-dependent electric field. As a result of birefringence, $LiNbO_3$ has two different refractive indices: n_o, for ordinary waves, and n_e, for extraordinary waves. Here, in the numerical analysis, we prefer to use n_e, which is 2.138 in the wavelength interval of interest [28].

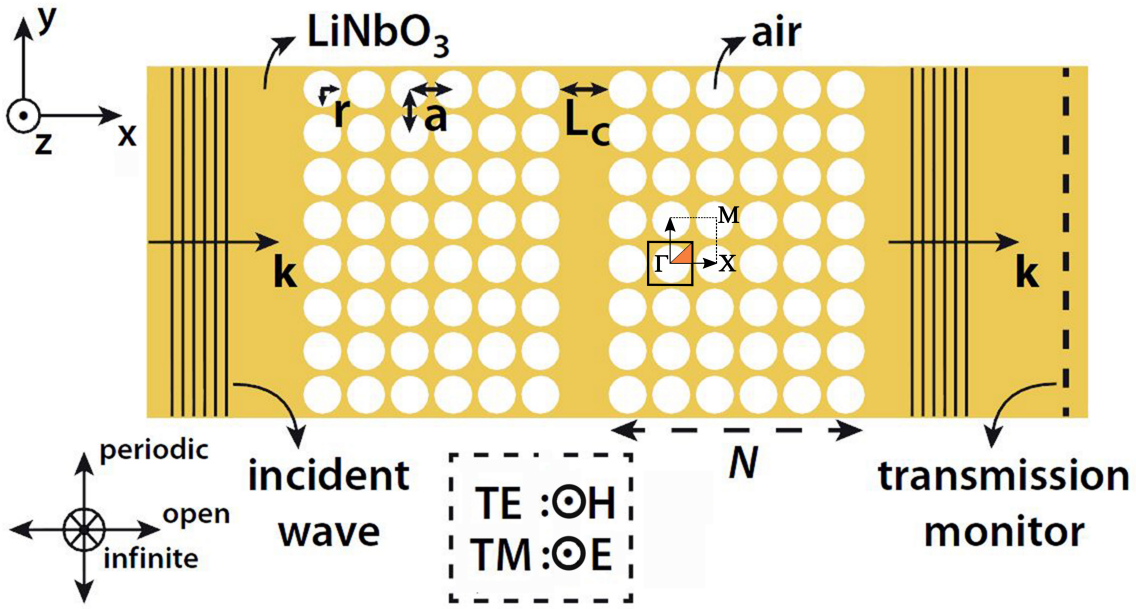

Figure 1. The cross-sectional view of the proposed Fabry–Perot cavity design. The PC structure is assumed to be periodic and infinitely long along the $y-$ and z-axis, respectively.

For the numerical analysis, the incident wave is defined as a plane wave that propagates in the $+x$ direction. In the practical realization stage, the plane wave field distribution can be approximated by coupling the incident light to a wide waveguide with the aid of a fiber. The calculation of the dispersion diagram and the group velocities is performed by utilizing the plane wave expansion (PWE) method [31]. The transmission spectrum is obtained by running finite-difference time-domain (FDTD) simulations (Photon Design, CrystalWave), in which one period of the corresponding structure is divided into 128 mesh cells for ensuring accurate data are obtained. In the FDTD simulations, periodic boundary conditions are implemented for the $\pm y$ directions and open boundary conditions are applied for the $\pm x$ directions to prevent the reflection of outgoing waves. Considering a sufficiently thick substrate, the calculations are realized in two dimensions. The main polarization state for operation is selected as TE polarization, for which the magnetic field is oriented along the z axis as shown in Figure 1.

3. Results and discussion

In the first step, we design a bulk square lattice PC in order to form a broad PBG region. One reason for working in the TE polarization is the possibility of the existence of a wider PBG region compared to the TM case. As

a design goal, we desire the PBG region to include $\lambda = 1.55$ μm, which is the chosen operation wavelength. Accordingly, we set the geometrical parameters for the bulk PC as $a = 530$ nm and $r/a = 0.4$. The cavity length, L_C, is calculated as $L_C = a - 2r = 106$ nm. The photonic band diagram and transmission spectrum are displayed in Figures 2a and 2b, respectively. According to Figure 2a, the bulk PC structure displays a PBG region between the normalized frequencies of $0.27(a/\lambda)$ and $0.39(a/\lambda)$ for the ΓX direction of wave-vectors. The transmission spectrum shown in Figure 2b confirms the existence of the PBG region and demonstrates that transmission is suppressed between approximately 1.3 μm and 1.9 μm.

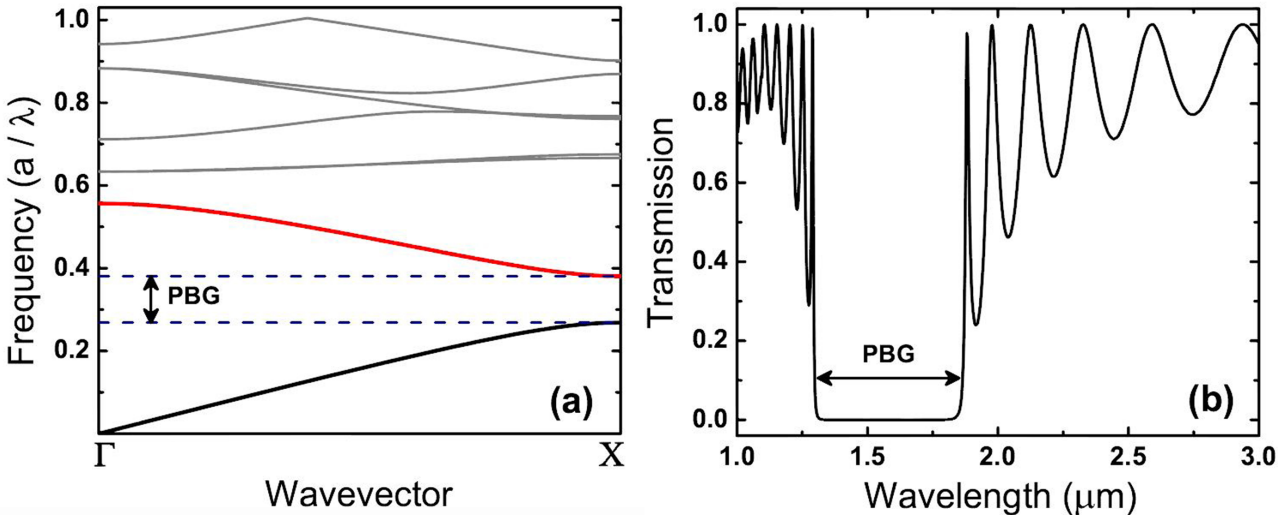

Figure 2. a) The dispersion diagram and b) transmission spectrum of the bulk PC structure. The black and red curves represent the lower and the upper band of the PBG region, respectively.

Next, we show the dispersion diagram and the transmission spectrum for the PC cavity geometry depicted in Figure 1 where $N = 6$. The corresponding dispersion diagram is shown in Figure 3a, where the mode arising due to the existence of the cavity is denoted by 'resonance band'. Figure 3b shows the transmission spectrum of the PC cavity between approximately 1.1 μm and 2.3 μm and Figure 3c is simply the enlarged view of the region enclosed by a dashed rectangle in Figure 3b. Figure 3c reveals that the transmission resonance occurs in the close vicinity of 1.55 μm and the normalized peak power transmission is approximately 0.89. We calculate the quality factor of the cavity from the ratio of the resonance frequency to FWHM-bandwidth as $Q \approx 1275$ for this spectrum. As it can be noted from Figure 3a, the ΓM direction presents a flat cavity resonance band that results in propagation with low group velocity, which is desirable for the enhancement of the electro-optic modulation effect. The group velocity of the resonance band is calculated as $0.0189\,c$ (c, the speed of light in vacuum) from the slope of the dispersion curve, which will later be used in the analysis of the electro-optic effect.

It has been stated that the bulk PC sections act as highly reflective blocks. Q and the transmission spectrum are strongly dependent on the reflectivity of the PC sections surrounding the cavity region and, therefore, N. In order to reveal this strong relation, the characteristics of the PC sections are changed by altering N from 5 to 7. Figure 4 shows the evolution of the transmission spectrum of the PC cavity for the above mentioned N values. It is observed that Q increases with increasing N, whereas the peak transmission at the cavity resonance decreases, since the reflectivity of the cavity mirrors increases with increasing N. Meanwhile, the spectral position of the cavity resonance is not modified because of the fact that L_C is kept

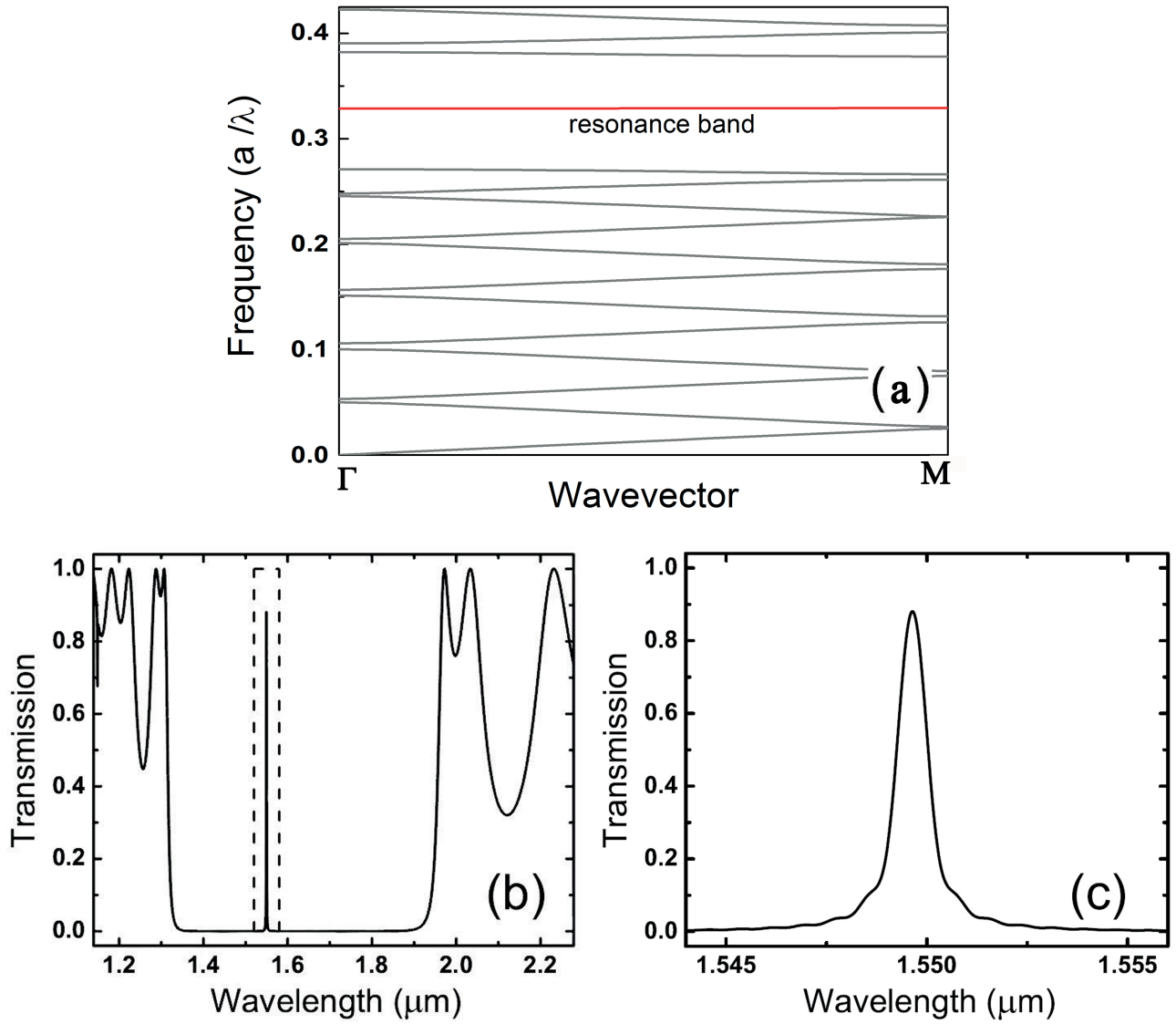

Figure 3. a) Dispersion diagram of the proposed Fabry–Perot-type cavity, b) transmission spectrum of the structure, (c) the enlarged view of the spectral behavior of the cavity resonance.

constant. Q values of the cavity resonances are evaluated as 455 and 4340, while the normalized peak power transmissions are 0.94 and 0.81 for $N = 5$ and $N = 7$, respectively.

The field distributions for the $N = 5$, $N = 6$, and $N = 7$ cases at the wavelengths where the transmission of the cavity mode is maximum are analyzed and the results are shown in Figure 5. The optical field highly concentrates inside and in the vicinity of the cavity region. The effective electro-optic coefficient in a structured material depends on the local field factor [29]. The local field factor, f, is defined by

$$f = \sqrt{\vartheta_G^{bulk}/\vartheta_G^{PC}}, \tag{1}$$

where ϑ_G^{bulk} and ϑ_G^{PC} are the group velocities inside the bulk and photonic crystal $LiNbO_3$, respectively. The group velocities at the cavity peak resonance frequencies are calculated as $0.0535\,c$, $0.0189\,c$, and $0.0099\,c$ for

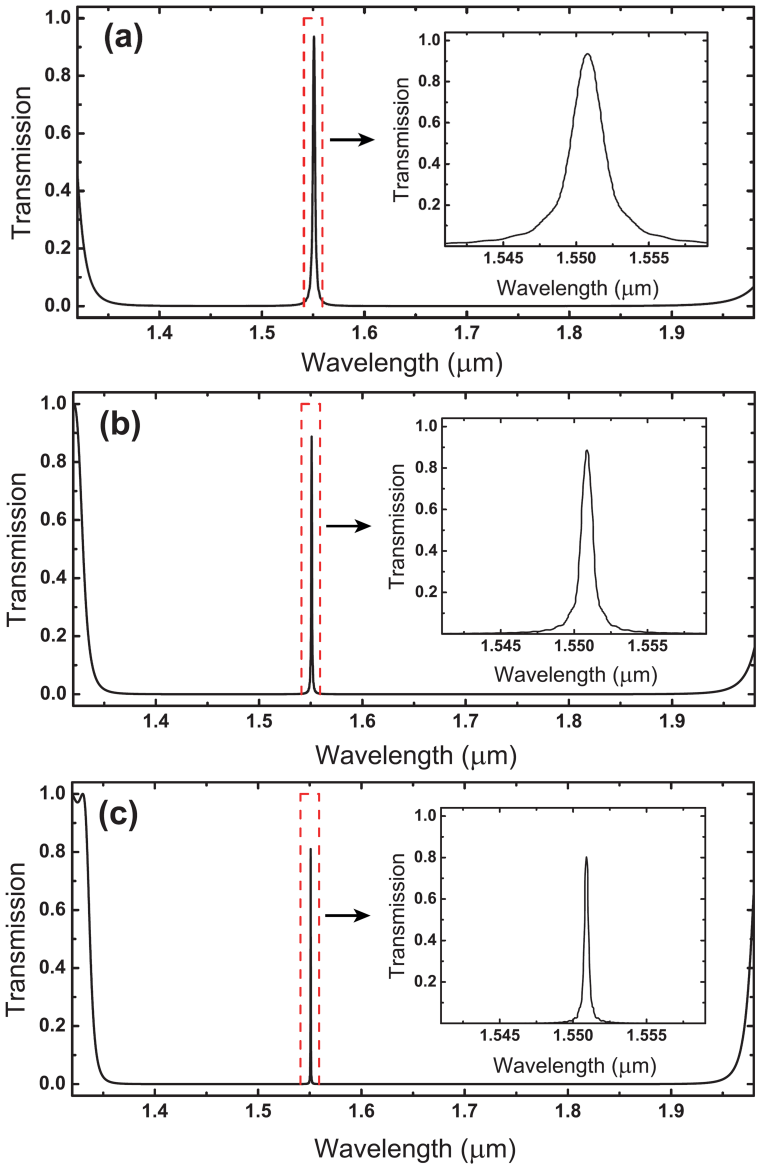

Figure 4. Output transmission spectra of the Fabry–Perot cavities for the cases of a) $N = 5$, b) $N = 6$, and c) $N = 7$. The enlarged views of the spectral behavior of the cavity resonances are shown in the insets.

$N = 5$, $N = 6$, and $N = 7$, respectively. Following Eq. (1), the local field factors are approximately 3, 5, and 7 for $N = 5$, $N = 6$, and $N = 7$, respectively. These calculated values of f and normalized peak power transmissions are observed to be higher than those for the PC based Fabry–Perot cavity with triangular lattice of holes in a $LiNbO_3$ background, where $r/a = 0.35$ [28]. Consistent with the increase in f as a function of N, it is obvious from Figure 5 that the magnetic field localizes more in the cavity center as N increases. Finally, as shown in Figure 5, the localized fields inside the cavity region have an approximately uniform distribution similar to what is observed in a traditional Fabry–Perot resonator. The PC cavity configuration with $N = 6$ is used for the rest of the analysis due to its good compromise between the peak power transmission and Q.

The evolution of the transmission spectrum with respect to changes in the refractive index of the cavity region, Δn, is analyzed in Figure 6. In the practical realization stage, the modification of n corresponds to

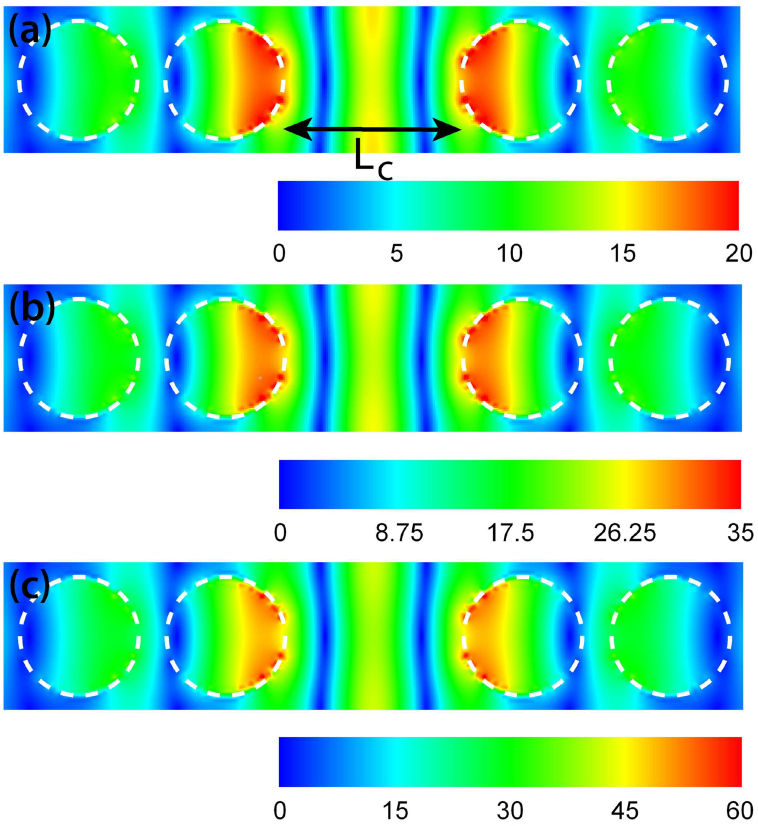

Figure 5. Magnetic field distributions of the Fabry–Perot cavities for the cases of a) $N = 5$, b) $N = 6$, and c) $N = 7$.

the application of an external static field. In other words, in this context, we model the electro-optic effect by modifying the refractive index. It has been shown that the effective modulation of the refractive index, n, in structures having strongly localized fields can be expressed as follows [29]:

$$\Delta n = -\frac{1}{2} n_e^3 r_{33} f^3 \frac{V}{L}, \tag{2}$$

where r_{33}, V, and L denote the electro-optic coefficient of $LiNbO_3$ (30 pm/V at 1.55 μm for $LiNbO_3$ [28]), the applied voltage, and the distance between the electrodes, respectively. Eq. (2) elucidates that the refractive index variation in the presence of external voltage increases by a factor of f^3 inside the PC medium with respect to the bulk electro-optic material. Our design of a Fabry–Perot-type $LiNbO_3$– based PC cavity shows a 123 times enhanced electro-optic effect compared to the bulk $LiNbO_3$.

The refractive index of the photonic crystal substrate is altered in linear increments of 0.05 that corresponds to an application of 23.6 V externally. The relationship between Δn and the peak transmission wavelength of the cavity mode, as illustrated in Figure 6a, reveals that the designed Fabry–Perot cavity has a high refractive index sensitivity and hence a high electro-optic modulation sensitivity. The amount of average redshift in the peak transmission wavelength is evaluated as approximately 28 nm per 0.05 increase in the refractive index, leading to a refractive index sensitivity of 558.95 nm/RIU or an electro-optic modulation sensitivity of 1.2 nm/V. Figure 6b shows the shift of the resonance wavelength as a function of refractive index change resulting from electro-optic modulation with the error bars representing the fluctuations in the wavelength shift

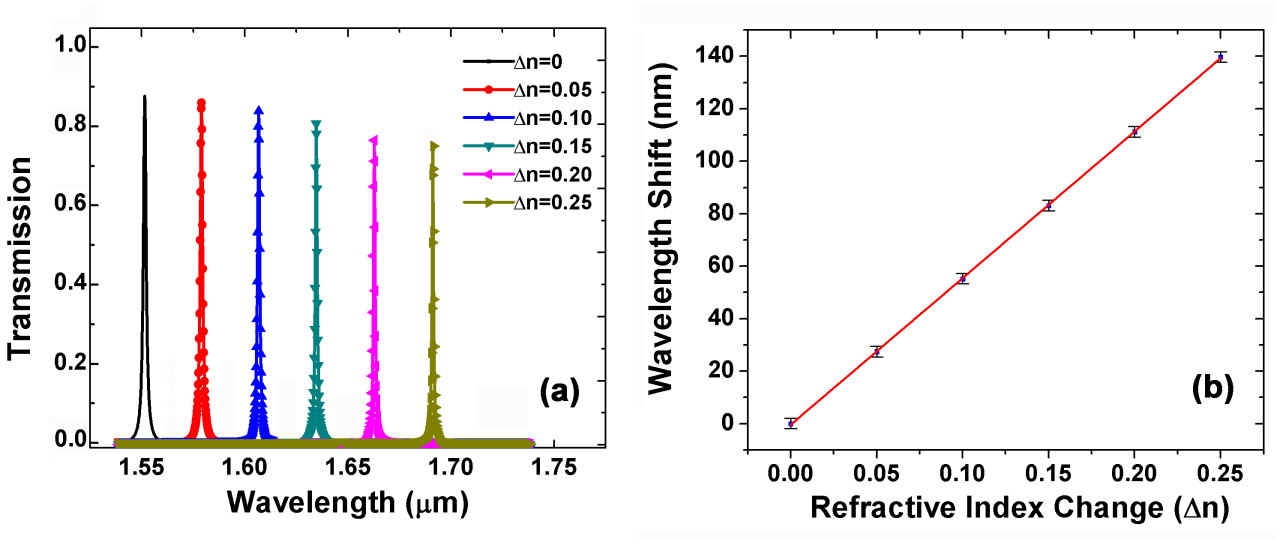

Figure 6. a) Demonstration of the wavelength modulation of the cavity resonances by altering the refractive index of the PC substrate, b) shift of the cavity resonance wavelength as a function of refractive index change.

that originate from 5 nm standard deviation of the holes from their correct positions in the square lattice. The alteration of the refractive index does not appreciably affect the value of peak power transmission. The shift of the resonance wavelength shows a linear relationship with the change of the refractive index and hence with the applied voltage (see Eq. (2)) and, therefore, the proposed structure can be a good candidate for practical applications that demand the enhancement of the electro-optic effect.

Following the investigation of the effect of refractive index modulation on the transmission spectrum, different possible functionalities of the proposed geometry, such as dual-mode and dual-polarization operation regimes, are reported. It is known that L_C determines the spectral position and the interdistance between the consecutive allowed modes of a Fabry–Perot cavity. In the analysis of the dual-mode regime, we do not modify the geometrical parameters other than L_C. For this particular Fabry–Perot cavity geometry, it is required for the observed cavity resonances to lie inside the PBG region of the corresponding PC structure. In the initial design, for which $a = 530$ nm, $r/a = 0.4$ and $L_C = 106$ nm, L_C has been carefully selected with the purpose of supporting only one cavity mode inside the PBG region. Nonetheless, by solely increasing L_C, we can expect the number of the supported cavity modes inside the PBG region to increase as a result of decreasing interdistance between consecutive modes. For this reason, L_C is arranged as 610 nm by enlarging the width of the cavity region. In this case, as predicted, the PBG region supports two distinct cavity modes at different wavelengths. Figure 7a demonstrates the occurrence of the two cavity modes that are denoted by 'resonance bands'. The transmission spectrum given in Figure 7b reveals the occurrence and the excitation of the two high transmission and high Q cavity modes. The peak normalized power transmission values are approximately given by 0.95 for the mode at $\lambda_0 = 1.36$ μm and 0.85 for the mode at $\lambda_0 = 1.65$ μm. Lastly, we calculate the Qs as 680 for the mode at $\lambda_0 = 1.36$ μm and 2870 for the mode at $\lambda_0 = 1.65$ μm.

Finally, we analyze the possibility of the simultaneous achievement of a high transmission and a large Q for both TE and TM polarizations. For the geometrical parameters that have been used in the single-polarization case, the resultant PBG regions for TE and TM waves do not overlap and, as a consequence, the resonance frequencies for TE and TM polarizations are significantly different. For enabling the achievement of two resonances that are fairly close to each other in terms of wavelength, we modify the aforementioned

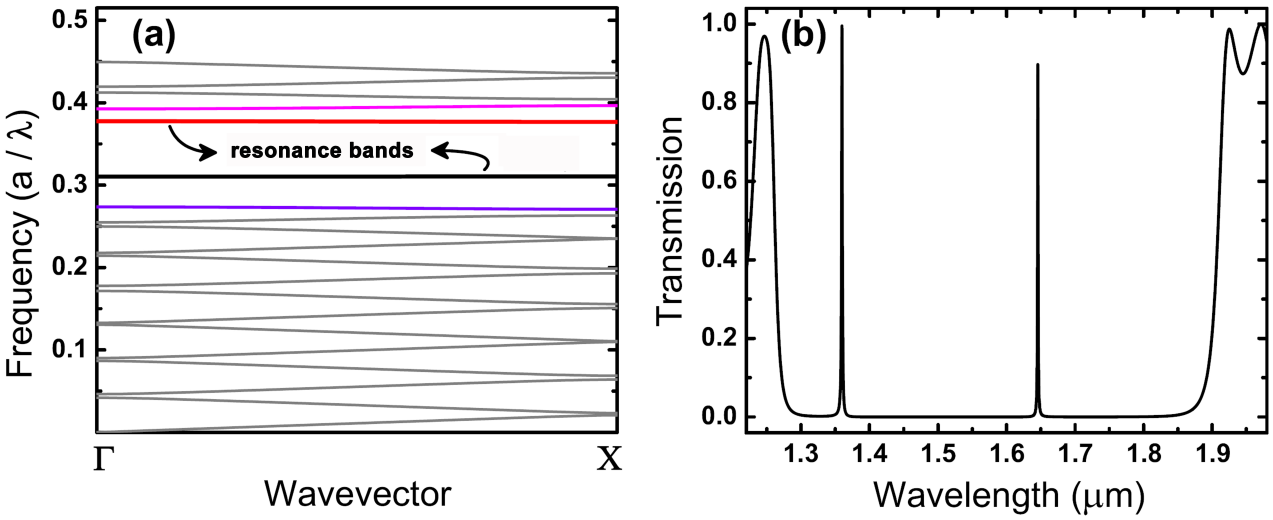

Figure 7. a) Dispersion diagram and b) transmission spectrum for the dual mode operation of the Fabry–Perot cavity. The arrows point to the resonance bands in the PBG.

geometrical parameters. The parameters used for the analysis of the dual-polarization regime are given by a = 520 nm and r/a = 0.46. For these parameters, we calculate $L_C = a - 2r$ = 41.6 nm. The reasoning behind this modification is the enabling of the PBG regions for TE and TM waves to coincide. Correspondingly, Figure 8 shows the transmission spectrum and the cavity resonances for TE and TM polarization states. Since the effective refractive index decreases when the radii of the holes are increased, the resonance wavelength of the TE mode shifts blue with a normalized peak power transmission of 0.89 at λ_0 = 1.5 μm. The normalized peak power transmission for the TM mode is obtained at λ_0 =1.6 μm with a transmission value of 0.96. The distinction between the spectral positions of the cavity resonances for TE and TM cases can be qualitatively explained by noting that different polarization states can encounter different cavity mirror reflectivity and, in turn, the propagation constants at the cavity mode wavelength can differ for TE and TM waves, so that the phase gained for TE and TM waves in a round-trip can be different. Q values are evaluated as 1394 and 340 for the TE and TM modes, respectively. From the viewpoint of practical applicability, it is advantageous that both of the cavity resonances yield high peak power transmissions and Qs.

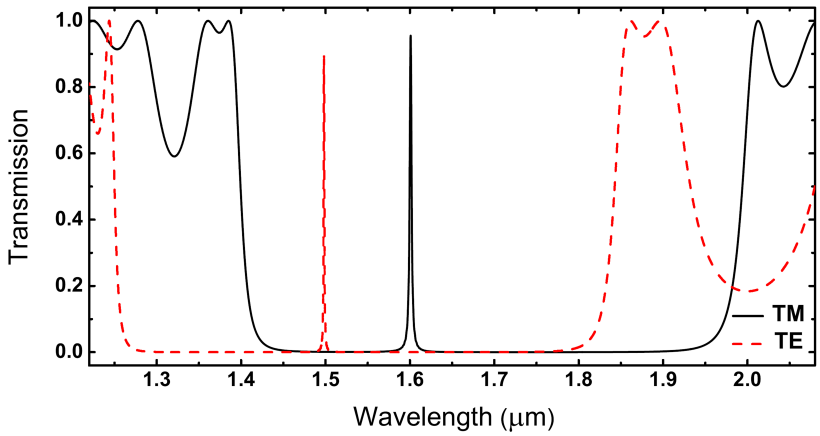

Figure 8. Transmission spectrum of the proposed Fabry–Perot-type cavity for dual polarization illumination.

4. Conclusions

We have proposed a Fabry–Perot-type cavity with side mirrors that are formed by air-hole photonic crystal structure to create high-transmission and high quality factor cavity resonances for efficient electro-optical modulation devices. A good compromise between the quality factor and peak power transmission is found for six rows of holes surrounding the cavity. The nearly uniform and high localization of the field at the cavity center is explained by the slow light effect, which sustains a localized mode with very low group velocity ($0.0189\,c$) at the cavity resonance frequency. The electro-optic effect is enhanced by 123-fold in the designed PC cavity as compared to that for the bulk $LiNbO_3$ as a consequence of the slow light effect. This enhancement is manifested with a large shift of the transmission band upon low voltage modulation that gives a sensitivity of 1.2 nm/V. Moreover, a dual mode regime with high normalized peak power transmissions and quality factors of the cavity resonances is presented by only changing the cavity length of the corresponding PC geometry. Finally, by changing the lattice unit and the holes' radius, the simultaneous use of the cavity for both TE and TM polarizations is demonstrated, which can be employed in polarization insensitive devices. The exploitation of the slow light effect in photonic crystal cavity structures with external tunability can facilitate micro- and nanoscale low power demanding active photonic devices.

Acknowledgments

This work was supported by the projects State Planning Organization (DPT-HAMİT), European Science Foundation (ESF-EPIGRAT), European Union (EU-N4E), and NATO-SET-181, and the Scientific and Technological Research Council of Turkey (TÜBİTAK) under the Project Nos. 107A004, 107A012, and 109E301. Two of the authors (F Bağcı and B Akaoğlu) acknowledge support from the Scientific Research Projects of Ankara University under the Project no. 16B0443005. E Özbay also acknowledges partial support from the Turkish Academy of Sciences.

References

[1] Yablonovitch, E.; Gmitter, T. J.; Meade, R. D.; Rappe, A. M.; Brommer, K. D.; Joannopoulos, J. D. *Phys. Rev. Lett.* **1991**, *67*, 3380-3383.

[2] Özbay, E.; Tuttle, G.; McCalmont, J. S.; Sigalas, M.; Biswas, R.; Soukoulis, C. M.; Ho, K. M. *Appl. Phys. Lett.* **1995**, *67*, 1969-1971.

[3] Vahala, K. J. *Nature* **2003**, *424*, 839-846.

[4] Akahane, Y.; Asano, T.; Song, B. S.; Noda, S. *Nature* **2003**, *425*, 944-947.

[5] Asano, T.; Song, B. S.; Noda, S., *Opt. Express* **2006**, *14*, 1996-2002.

[6] Srinivasan, K.; Barclay, P. E.; Borselli, M.; Painter, O. *Phys. Rev. B* **2004**, *70*, 081306.

[7] Painter, O.; Lee, R. K.; Scherer, A.; Yariv, A.; O'Brien, J. D.; Dapkus, P. D.; Kim, I. *Science* **1999**, *284*, 1819-1821.

[8] Khitrova, G.; Gibbs, H. M.; Jahnke, F.; Kira, M.; Koch, S. W. *Rev. Mod. Phys.* **1999**, *71*, 1591-1639.

[9] Park, H. G.; Barrelet, C. J.; Wu, Y.; Tian, B.; Qian, F.; Lieber, C. M. *Nat. Photon.* **2008**, *2*, 622-626.

[10] Michler, P.; Kiraz, A.; Becher, C.; Schoenfeld, W. V.; Petroff, P. M.; Zhang, L.; Hu, E.; Imamoglu, A. *Science* **2000**, *290*, 2282-2285.

[11] Song, B. S.; Noda, S.; Asano, T. *Science* **2003**, *300*, 1537.

[12] Spillane, S. M.; Kippenberg, T. J.; Vahala, K. J. *Nature* **2002**, *415*, 621-623.

[13] Soljacic, M.; Joannopoulos, J. D. *Nat. Mater.* **2004**, *3*, 211-219.

[14] Lu, H.; Baida, F. I.; Ulliac, G.; Courjal, N.; Collet, M.; Bernal M. P. *Appl. Phys. Lett.* **2012**, *101*, 151117.

[15] Shambat, G.; Ellis, B.; Mayer, M. A.; Majumdar, A.; Haller, E. E.; Vuckovic, J. *Opt. Express* **2011**, *19*, 7530-7536.

[16] Roussey, M.; Bernal, M. P.; Courjal, N.; Van Labeke, D.; Baida, F. I. *Appl. Phys. Lett.* **2006**, *89*, 241110.

[17] Burr, G.W.; Diziain, S.; Bernal, M. P. *Opt Express* **2008**, *16*, 9, 6302-6316.

[18] Zhao, Q. Z.; Zhang, Z. B.; Xu, J. Q.; Wong, W. H.; Yu, D. Y.; Yue-Bun Pun, E.; Zhang, D. L. *Mater. Chem. Phys.* **2017**, *186*, 498-504.

[19] Lim, S. T.; Ang, T. Y. L.; Png, C. E.; Deng, J.; Danner, A. J. In *SPIE Proceedings: Optical Components and Materials XIII*, **2016**, *9744*, 974413-1-7.

[20] Song, B. S.; Noda, S.; Asano, T.; Akahane, Y. *Nat. Mater.* **2005**, *4*, 207-210.

[21] Arita, M.; Ishida, S.; Kako, S.; Iwamoto, S.; Arakawa, Y. *Appl. Phys. Lett.* **2007**, *91*, 051106.

[22] Deotare, P. B.; McCutcheon, M. W.; Frank, I. W.; Khan, M.; Lončar, M. *Appl. Phys. Lett.* **2009**, *94*, 121106.

[23] Beaky, M. M.; Burk, J. B.; Everitt, H. O.; Haider, M. A.; Venakides, S. *IEEE T. Microw. Theory* **1999**, *47*, 11, 2085-2091.

[24] Cecelja, F.; Bordovsky, M.; Balachandran, W. *IEEE T. Instrum. Meas.* **2001**, *50*, 2, 465-469.

[25] Rolland Q., Dupont S., Gazalet J., Kastelik J. C., Pennec Y., Djafari-Rouhani B., Laude V. *Opt. Express* **2014**, *22*, 13, 16288-16297.

[26] Wang, Y.; Zhou, S.; He, D.; Hu, Y.; Chen, H.; Liang, W.; Yu, J.; Guan, H.; Luo, Y.; Zhang, J.; et al. *Opt. Lett.* **2016**, *41*, 20, 4739-4742.

[27] Lu, H.; Sadani, B.; Ulliac, G.; Courjal, N.; Guyot, C.; Merolla, J. M.; Collet, M.; Baida, F. I.; Bernal, M. P. *Opt. Express* **2012**, *20*, 19, 20884-20893.

[28] Lu, H.; Sadani, B.; Courjal, N.; Ulliac, G.; Smith, N.; Stenger, V.; Collet, M.; Baida, F. I.; Bernal, M. P. *Opt. Express* **2012**, *20*, 2974-2981.

[29] Roussey, M.; Baida, F. I.; Bernal, M. P. *J. Opt. Soc. Am. B* **2007**, *24*, 6, 1416-1422.

[30] Basseras, P.; Dwayne Miller, R.; Gracewski, S. M. *J. Appl. Phys.* **1991**, *69*, 7774-7781.

[31] Johnson, S.; Joannopoulos, J. *Opt. Express* **2001**, *8*, 173-190.